# 11.2 LARGE EDDY SIMULATION SENSITIVITY EXPERIMENTS OF THE ASTEX STRATOCUMULUS TO CUMULUS TRANSITION

J.J. van der Dussen[1]*, S.R. de Roode[1] and A.P. Siebesma[2,1]
[1]Delft University of Technology, Delft, The Netherlands
[2]Royal Netherlands Meteorological Institute, Delft, The Netherlands

**Abstract**

**A diagnostic equation for the tendency of the liquid water path (LWP) of a stratocumulus cloud layer is derived. This equation allows the total LWP tendency to be split into the contributions due to entrainment, cloud base turbulent fluxes of heat and moisture, radiation, precipitation and large scale divergence. The equation is used to analyse the results of the ASTEX stratocumulus to cumulus transition as simulated using the Dutch Atmospheric Large Eddy Simulation. It is shown that the contribution to the LWP of the turbulent flux at cloud base, which is mainly due to transport by cumulus clouds, increases during the transition, thereby extending the stratocumulus lifetime. Entrainment fluxes at the inversion, however, also increase, such that overall the cloud layer gradually thins.**
**Sensitivity experiments are furthermore performed in order to test earlier hypotheses, stating that a decrease of the large scale divergence leads to an earlier break up of the cloud layer. The results confirm recent research that contradicts the hypotheses, by showing a delayed cloud break up for lower values of the large scale divergence.**
**It is shown that, despite the higher degree of decoupling of the mean state vertical profiles in the cases with lower subsidence, the contribution of cloud base turbulent fluxes to the LWP tendency is higher compared to cases with higher large scale divergence.**

## 1. INTRODUCTION

As a result of the Hadley circulation, fields of stratocumulus clouds typically form over mid-latitudinal oceans. As these cloud fields are advected towards the equator by the trade winds, they are subjected to increasing sea surface temperatures, causing the atmospheric boundary layer to deepen. Gradually, the stratocumulus clouds are replaced by shallow cumuli, causing a significant drop in the area averaged albedo. During the cloud transition, both cloud types coexist, which makes their parametrisation particularly challenging.
The first field experiment particularly aiming at a better understanding of these transitions is the Atlantic Stratocumulus Transition EXperiment (ASTEX, Albrecht et al., 1995), which took place in June 1992. During the experiment, two Lagrangian measurement series were performed, the first of which contained an almost complete transition from a shallow, relatively well-mixed stratocumulus layer to a deeper boundary layer dominated by shallow cumuli, with only a thin patch of broken stratocumulus at the top (Bretherton et al., 1995; Bretherton and Pincus, 1995; De Roode and Duynkerke, 1996, 1997).
Since then, the ASTEX experiment has been the topic of many modelling studies. The GEWEX Cloud System Study (GCSS) working group organised two 3D Large Eddy Simulation (LES) model intercomparison cases based on the second (A209) and the third (RF06, Duynkerke et al., 1999) measurement flights of the first Lagrangian. Both flights took place in a solid, relatively well-mixed stratocumulus layer during the night. The simulations lasted only 3 hours, because of the limited available computational power. Additionally, in another GCSS effort the entire first Lagrangian was modelled using several 1D and 2D turbulence models (Bretherton et al., 1999).
Svensson et al. (2000) used the set-up of this model intercomparison case to perform several sensitivity studies using a 1D turbulence model, from which they conclude that the main driver of the transition is the increase in the sea surface temperature. They furthermore show that, when the large scale subsidence rate is decreased, the stratocumulus life-time is prolonged and the liquid water path is on average higher throughout the transition.
More recently, Sandu et al. (2010) analysed satellite data of many Lagrangian trajectories in which stratocumulus to cumulus transitions occur. They constructed three sets of initial and boundary conditions by ordering the cases on the basis of the transition pace. Owing to the increase in computational resources, these cases could be simulated using a LES model (Sandu and Stevens, 2011). The results show that LES models are capable of representing the general features (such as the gradual deepening of the boundary layer, the occurrence of cumulus under stratocumulus and the thinning and eventually breaking up of the stratocumulus cloud layer) of these cloud transitions very well.
A revised ASTEX Lagrangian 1 set-up has recently been proposed (together with the three composite transition cases) to be run by LES models and single column models as a joint GEWEX Atmospheric System Study (GASS)/EUCLIPSE (European Union Cloud Intercomparison, Process Study & Evaluation Project) effort to further advance the understanding of cloud transitions and to evaluate the performance of models against observations. The comparison of the LES model results with the observations for ASTEX is the topic of a paper by Van der

* *Corresponding author address:* Johan van der Dussen, Delft University of Technology, Delft, The Netherlands (J.J.vanderDussen@tudelft.nl)

Dussen et al. (in preparation, DR12 hereafter).
The goal of this conference proceeding is, in the first place, to introduce a tendency equation for the cloud liquid water path (LWP) of the stratocumulus cloud at the top of the boundary layer, which is then used to analyse some of the important aspects of the ASTEX transition as simulated using the Dutch Atmospheric LES (DALES, Heus et al., 2010).
Secondly, similar to Svensson et al. (2000), several additional simulations are performed, using different prescribed large scale subsidence rates. The motivation for these experiments originates in the uncertainty of the available measurements (Bretherton et al., 1999; Ciesielski et al., 1999) and the large spacial and temporal variability of the reanalysis data for this variable. The LWP tendency equation is then used to shed light on the cause of the prolonging effect that a decrease of the subsidence rate has on the transition (De Roode and Van der Dussen, 2010; Sandu and Stevens, 2011; Svensson et al., 2000).
The contents of this conference proceeding are as follows: Section 2 contains the derivation of the liquid water path tendency equation, which is used in Section 3 to aid in the understanding of the response of the transition to a perturbed large scale divergence. Section 4 contains a summary of the main conclusions as well as some discussion.

## 2. LIQUID WATER PATH TENDENCY EQUATION

In this section, an equation for the tendency of the liquid water path of the stratocumulus cloud is derived. The terms in this equation are then split in order to determine the relative importance of each of the individual physical processes on the evolution of the LWP.
At the basis of this analysis is the work of Randall (1984), who derived an analytical expression for the combinations of temperature and humidity inversion jumps, for which entrainment acts to deepen the cloud layer, instead of thinning it by drying and warming the layer. Here, a similar analysis is applied to the stratiform cloud layer at the top of the boundary layer.
Following the model of Park et al. (2004) and Wood and Bretherton (2004), the stratocumulus layer is assumed to be well-mixed, which is supported by the shape of the hourly averaged total humidity $q_T$ and liquid water potential temperature $\theta_L$ vertical profiles during the ASTEX Lagrangian transition. Under this assumption, the liquid water content at the boundary layer top $q_{L,\text{top}}$ can be related to the depth of the stratocumulus cloud layer $h_c$, via a $q_L$ lapse rate $\Gamma_{q_L}$:

$$q_{L,\text{top}} \approx \frac{\partial q_L}{\partial z}\left(z_i - z_b\right) = \Gamma_{q_L} h_c. \tag{1}$$

For the rate of change of $h_c$, the following can then be written:

$$\frac{\partial h_c}{\partial t} = \frac{1}{\Gamma_{q_L}}\frac{\partial q_{L,\text{top}}}{\partial t} + q_{L,\text{top}}\frac{\partial}{\partial t}\left(\frac{1}{\Gamma_{q_L}}\right). \tag{2}$$

The second term on the rhs describes changes in the cloud thickness due to changes in the lapse rate of $q_L$. In a saturated environment, this lapse rate can be written as:

$$\Gamma_{q_L} = -\frac{\partial q_s}{\partial z}, \tag{3}$$

for which an expression is derived in Appendix B. A plot of the variation of $\partial q_s/\partial z$ with temperature and pressure is shown in Figure A-1c.
The variation of $\Gamma_{q_L}$ with time is assumed to be small, such that Eq. (2) reduces to:

$$\frac{\partial h_c}{\partial t} = \frac{1}{\Gamma_{q_L}}\frac{\partial q_{L,\text{top}}}{\partial t}. \tag{4}$$

Since the cloud layer is assumed to be well-mixed, $q_{L,\text{top}}$ is a function of the humidity and liquid water potential temperature in the stratocumulus layer, respectively $q_{T,\text{cld}}$ and $\theta_{L,\text{cld}}$, and of the inversion height $z_i$:

$$q_{L,\text{top}} = f(q_{T,\text{cld}}, \theta_{L,\text{cld}}, z_i). \tag{5}$$

The pressure at the surface is kept constant and hydrostatic equilibrium is assumed, such that there is no explicit dependency of $q_{L,\text{top}}$ on pressure. Note furthermore that $q_{L,\text{top}}$ is no function of cloud base height $z_b$ explicitly, as the depth of the cloud layer is fixed by its thermodynamic state through $\Gamma_{q_L}$.
Following Randall (1984), partial differentiation is used to write:

$$\frac{\partial q_{L,\text{top}}}{\partial t} = \left(\frac{\partial q_L}{\partial q_T}\right)_{\theta_L,z_i}\frac{\partial q_{T,\text{cld}}}{\partial t} + \left(\frac{\partial q_L}{\partial \theta_L}\right)_{q_T,z_i}\frac{\partial \theta_{L,\text{cld}}}{\partial t} + \left(\frac{\partial q_L}{\partial z_i}\right)_{\theta_L,q_T}\frac{\partial z_i}{\partial t}, \tag{6}$$

in which the variables in the subscripts are kept constant in the derivative and all derivatives are implicitly assumed to be evaluated at cloud top.
For the partial derivatives of $q_L$ with respect to $q_T$ and $\theta_L$, the following expressions can be derived (see Appendix A):

$$\left(\frac{\partial q_L}{\partial q_T}\right)_{\theta_L,z_i} = \eta; \tag{7a}$$

$$\left(\frac{\partial q_L}{\partial \theta_L}\right)_{q_T,z_i} = -\Pi\gamma\eta. \tag{7b}$$

Here, $\gamma$ is the change of the saturation specific humidity with temperature, which can be evaluated using the Clausius-Clapeyron relation in Eq. (A-6). Furthermore, $\Pi$ is the Exner function and $\eta$, defined by Eq. (A-9), can be interpreted as an efficiency at which $q_T$ is converted to $q_L$. This efficiency is plotted as a function of temperature for a relevant range of pressures in Figure A-1a. For the stratocumulus layer as observed during ASTEX, $\eta \approx 0.4$. The fact that an increase in $q_T$ leads to a significantly smaller increase in $q_L$, is mainly due to the heating of a parcel as water condensates. Keeping $\theta_L$, which is usually approximated as:

$$\theta_L = \theta - \frac{L_v}{\Pi c_p} q_L, \tag{8}$$

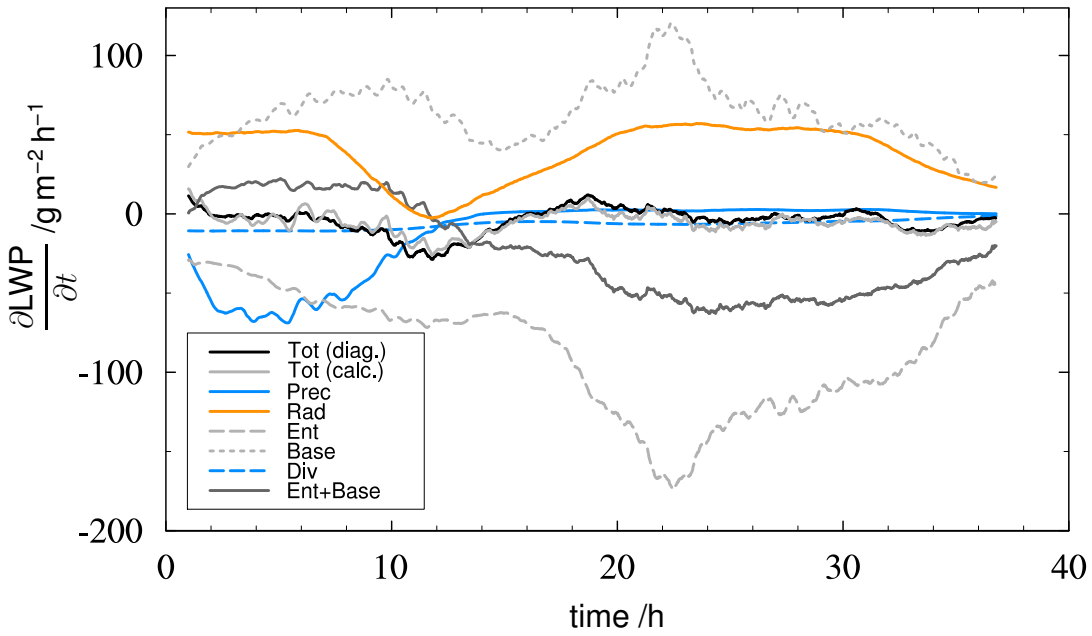


**FIG. 1:** Timeseries the LWP tendency for the ASTEX stratocumulus to cumulus transition as simulated using the Dutch Atmospheric LES. The total tendency of the LWP as calculated directly from $q_L$ profiles is indicated by the solid black line, while the solid light grey line indicates the total tendency found by taking the sum of the contributions of each of the processes according to Eq. (20). The terms in the legend refer to those introduced in Eq. (21).

constant, implies a balance between the change in $q_L$ and the associated heat release/uptake, which results in $0 < \eta < 1$.

Equations (7) and (B-1) can be used to substitute out the partial derivatives in Eq. (6). For the tendencies of $q_T$ and $\theta_L$ in this latter equation, the conservation equations can be written as follows:

$$\frac{\partial \varphi}{\partial t} = -\frac{\partial \overline{w'\varphi'}}{\partial z} + \frac{\partial S_\varphi}{\partial z}. \tag{9}$$

The diabatic processes, for which a variable $\varphi$ is not conserved, are included through $S_\varphi$. For the given choice of variables, these processes are: longwave and shortwave radiation and precipitation.

In case of a well-mixed cloud layer, the turbulent flux divergence in Eq. (9) can be written as follows:

$$\begin{aligned} -\frac{\partial \overline{w'\varphi'}}{\partial z} &= -\frac{1}{h_c}\left(\overline{w'\varphi'}_{\text{top}} - \overline{w'\varphi'}_{\text{base}}\right) \\ &= \frac{1}{h_c}\left(r_\varphi \overline{w'\varphi'}_{\text{surf}} + w_e \Delta_{\text{i}}\varphi\right). \end{aligned} \tag{10}$$

In this equation, $r_\varphi$ is the ratio of the turbulent flux of $\varphi$ at stratocumulus cloud base over that at the surface. This cloud base is defined as the lowest height at which the cloud fraction is greater than 0.7. This value is chosen rather arbitrary, but the results are quite insensitive to the choice, since the average cloud fraction decreases rapidly with height at the base of the stratocumulus layer. In order to rewrite the flux at cloud top in Eq. (10), the flux-jump relation:

$$\overline{w'\varphi'}_{\text{top}} = -w_e \Delta_{\text{i}}\varphi, \tag{11}$$

in which $\Delta_{\text{i}}\varphi$ denotes the inversion jump of variable $\varphi$, was used.

The tendency of $z_i$ in Eq. (6), is written as the sum of the entrainment rate and the mean vertical wind $\overline{w}$ at $z_i$:

$$\frac{\partial z_i}{\partial t} = w_e + \overline{w}(z_i). \tag{12}$$

After substitution of the above equations in Eq. (6) and after some rewriting, the following expression for the tendency in of the stratocumulus cloud depth can be found:

$$\begin{aligned} \frac{\partial h_c}{\partial t} = &-\frac{\Pi\gamma\eta}{\Gamma_{q_L} h_c}\left(r_{\theta_L}\overline{w'\theta'_L}_{\text{surf}} + w_e\Delta_{\text{i}}\theta_L + \Delta_{\text{c}}S_{\theta_L}\right) \\ &+\frac{\eta}{\Gamma_{q_L} h_c}\left(r_{q_T}\overline{w'q'_T}_{\text{surf}} + w_e\Delta_{\text{i}}q_T + \Delta_{\text{c}}S_{q_T}\right) \\ &+w_e - Dz_i. \end{aligned} \tag{13}$$

The diabatic terms have been rewritten by defining a difference over the stratocumulus cloud layer $\Delta_{\text{c}}$, such that:

$$\frac{\partial S_\varphi}{\partial z} = \frac{\Delta_{\text{c}} S_\varphi}{h_c}. \tag{14}$$

The emission of longwave radiation and the absorption of solar radiation can then be taken into account by writing:

$$\Delta_{\text{c}} S^{\text{rad}}_{\theta_L} = \frac{1}{\rho c_p}\left(\Delta_{\text{c}} F_{SW} + \Delta_{\text{c}} F_{LW}\right), \tag{15}$$

where $F_{SW}$ and $F_{LW}$ denote net fluxes of shortwave and longwave radiation respectively.

The removal of liquid water from the cloud layer in the form of precipitation, influences not only $q_T$ but also $\theta_L$,

as follows:

$$\Delta_c S_{q_T}^{\text{prec}} = \frac{\Delta_c F_p}{\rho L_v} \tag{16a}$$

$$\Delta_c S_{\theta_L}^{\text{prec}} = \frac{\Delta_c F_p}{\rho c_p}. \tag{16b}$$

In this equation, $F_p$ is the precipitation flux, in W m$^{-2}$. Equation (13) reveals an inverse dependency of the tendency of the cloud layer thickness to the cloud layer thickness itself. Using the definition of the LWP:

$$\text{LWP} = \int_{z=0}^{\infty} \rho q_L dz, \tag{17}$$

Eq. 13 can be simplified slightly. As earlier, for this case of a well-mixed stratocumulus cloud layer, a adiabatic lapse rate is assumed for $q_L$. When, furthermore, the $\rho$ is assumed to be constant with height, the definition above reduces to:

$$\text{LWP} = \frac{1}{2}\rho\Gamma_{q_L} h_c^2. \tag{18}$$

Now taking the derivative of both sides of this equation with respect to time gives:

$$\frac{\partial \text{LWP}}{\partial t} = \frac{1}{2}\frac{\partial}{\partial t}\left(\rho\Gamma_{q_L} h_c^2\right) \approx \rho\Gamma_{q_L} h_c \frac{\partial h_c}{\partial t}, \tag{19}$$

in which the variation of $\rho$ and $\Gamma_{q_L}$ with time is assumed to be small. Substituting this in Eq. (13) greatly simplifies the first two terms on the rhs slightly, but makes the last two terms more complex. The contributions of these latter two terms to the total LWP tendency, however, are rather small.

Finally, Eqs. (15) and (16) can be substituted into Eq. (13) and through reordering, the effects of five processes, namely cloud base turbulent fluxes ('Base'), entrainment ('Ent'), precipitation ('Prec'), radiation ('Rad') and divergence ('Div'), on the LWP tendency can be isolated to give:

$$\frac{\partial \text{LWP}}{\partial t} = \text{Base} + \text{Ent} + \text{Prec} + \text{Rad} + \text{Div} \tag{20}$$

in which

$$\text{Base} = \rho\eta\left(r_{q_T}\overline{w'q'_T}_{\text{surf}} - \Pi\gamma r_{\theta_L}\overline{w'\theta'_L}_{\text{surf}}\right), \tag{21a}$$

$$\text{Ent} = \rho\eta w_e\left(\Delta_i q_T - \Pi\gamma\Delta_i\theta_L\right) + \rho\eta h_c\Gamma_{q_L} w_e \tag{21b}$$

$$\text{Prec} = \eta\,\Delta_c F_p\left(\frac{1}{L_v} - \frac{\Pi\gamma}{c_p}\right), \tag{21c}$$

$$\text{Rad} = \frac{\eta}{c_p}\left(\Delta_c F_{SW} + \Delta_c F_{LW}\right), \tag{21d}$$

$$\text{Div} = \rho\eta h_c\Gamma_{q_L}\overline{w(z_i)}. \tag{21e}$$

Figure 1 shows time series of each of the terms in this equation for the ASTEX transition as described by DR12. The simulation was performed using DALES.

The total LWP tendency of the stratocumulus layer, calculated from the instantaneous $q_L$ profiles at an interval of 60 s is indicated by the black line. The sum of the individual terms in the LWP budget equation is given by the solid light grey line. The budget equation result shows excellent agreement with the actual tendency, which is somewhat unexpected considering the uncertainty in the determination of the inversion jumps of $q_T$ and $\theta_L$. The magnitudes of these jumps were diagnosed from the 60 s instantaneous profiles, by determining the levels at which the vertical gradient of the variable drops below a certain fraction of the maximum gradient.

Figure 1 shows that the contributions of the entrainment term and the term due to cloud base turbulent fluxes of $q_T$ and $\theta_L$ are large compared to the net tendency. The correlation between these two terms is high, which is not surprising, as increasing cloud base fluxes cause additional latent heat release in the cloud layer, which increases the production of turbulent kinetic energy and subsequently the entrainment. Similarly, much of the turbulent flux of moisture and heat at cloud base height is caused by downdrafts induced by entrainment of air from the free atmosphere.

As the sea surface temperature and consequently the surface latent heat flux increases, the thickening effect due to cloud base fluxes also increases. At the same time, the thinning due to entrainment becomes stronger, which is caused by the increase of the entrainment rate and the magnitude of the inversion jumps.

During the first day, the radiative contribution, indicated by the solid orange line in Figure 1, shows a clear minimum, even becoming slightly negative. This direct effect, caused by the heating of the cloud layer and the subsequent evaporation of the cloud, is also visible in the the total LWP tendency. As the liquid water path of the cloud layer decreases, the amount of precipitation also decreases rapidly, which acts as a buffering mechanism for the LWP, as it counteracts the strong change in the LWP tendency caused by shortwave radiation. Furthermore, as a result of the decreased turbulence intensity in the cloud layer during the day, the entrainment rate decreases, such that the cloud thinning due to entrainment stagnates, additionally buffering the direct effect of radiation on the LWP.

Another interesting effect of the absorption of solar radiation during the day is visible in the contribution of the cloud base fluxes of $q_T$ and $\theta_L$ to the LWP tendency. The decoupling of the boundary layer during the day (Bougeault, 1985; Turton and Nicholls, 1987) causes a decrease in this cloud thickening process. It reaches a minimum 15 h into the simulation, approximately 2 h after local noon. The turbulence decoupling of the boundary layer builds up slowly during the day, which introduces a time lag as compared to the radiative effect. Furthermore, due to this decoupling, moisture builds up in the subcloud layer. During the night, this moisture is transported to the cloud layer again, resulting in a peak in the cloud base flux contribution. At the same time, however, this additional transport also enhances the entrainment.

As an effect of the boundary layer decoupling, the contributions of the $q_T$ and $\theta_L$ fluxes at cloud base and

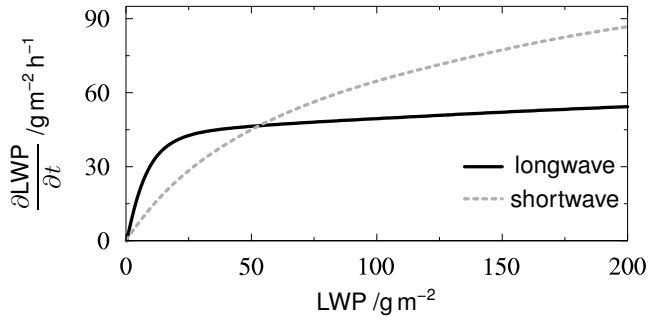


**FIG. 2:** The absolute LWP tendency caused by longwave (solid black) and shortwave radiation (dashed grey, absolute value). The calculations were performed using the initial conditions of the ASTEX model intercomparison case. By varying the boundary layer value of the total humidity, well-mixed stratocumulus profiles are obtained with a range of LWPs. The solar radiative fluxes are calculated at local noon, 13 UTC.

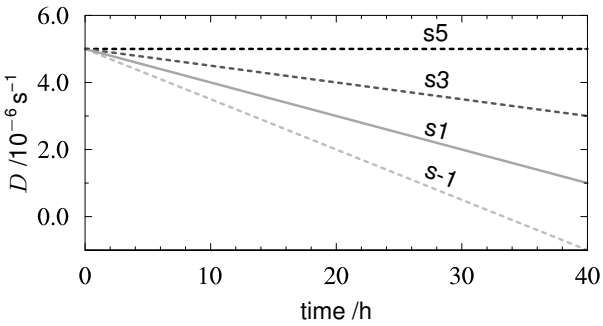


**FIG. 3:** Divergence as a function of time for the reference and the sensitivity simulations. The dashed lines are sensitivity experiments. The numbers indicate the values of the divergence at the end of the simulation.

of the entrainment flux, indicated by the solid grey line in Figure 1, becomes negative and even though the cloud base fluxes restore during the second night, the sum remains negative. These results indicate that the cloud thinning typical for stratocumulus to cumulus transitions is lead by turbulence.

Nevertheless, the transport of moisture by cumulus clouds is an important process causing the persistence of the stratocumulus layer throughout the transition. This is in line with the findings of Martin et al. (1995), who conclude on the basis of observations made during the ASTEX campaign, that the stratocumulus cloud layer is thicker at locations where cumulus clouds are found.

During the second night of the transition (hour 25 is at local midnight), the LWP tendency from radiation is back at approximately the same level as the first night, at about 50 g m$^{-2}$ h$^{-1}$. This value seems to be rather robust.

Figure 2 shows the absolute shortwave and longwave radiative tendencies, calculated using Eq. (21d), for a range of LWPs. This range is obtained by perturbing the boundary layer total humidity of the initial profiles. The radiative transfer calculations were done for the location of the ASTEX experiment at local noon, when the downwelling shortwave radiative flux is largest.

The figure shows that, as long as LWP $>$ 25 g m$^{-2}$, the contribution of longwave radiation is approximately constant. This due to the fact that emission of longwave radiation takes place in a very thin layer at the top of the stratocumulus layer. Therefore, at higher LWP, the cloud layer emits radiation approximately as a black body, independent of the depth of the layer. For LWP $<$ 25 g m$^{-2}$, the cloud thickening tendency drops of quickly and the stratocumulus cloud layer will rapidly vanish.

Absorption of shortwave radiation on the other hand, takes place over a larger cloud depth, such that the total amount of absorbed shortwave radiation decreases as the cloud thins. Over the whole range, the LWP tendency due to shortwave radiation decrease with LWP. For ASTEX at local noon, shortwave and longwave contributions fully cancel at a liquid water path of approximately 50 g m$^{-2}$.

In the second part of the transition, radiative cooling is the main process counteracting the cloud thinning due to turbulence decoupling (dotted dark grey line in Figure 1).

The remaining two effects in Figure 1 are those of precipitation and large scale divergence. The precipitation contribution is only significant in the first part of the transition, when precipitation fluxes are large. The thinning of the cloud during the day prohibits rain formation and causes its LWP tendency to become approximately zero, thereby damping the decrease of the net tendency caused by shortwave radiation.

The large scale divergence term, Eq. (21e), is small compared to the influence of the other processes, but not negligible compared to the net cloud thickness tendency. As stratocumulus clouds typically form in regions with large scale subsidence, $D > 0$, and the contribution to the LWP tendency is negative. During the ASTEX transition, it amounts to an average LWP decrease of approximately 6 g m$^{-2}$ h$^{-1}$.

## 3. DIVERGENCE SENSITIVITY

In this section, the sensitivity of the ASTEX transition to perturbations in the divergence are investigated. The reason for performing these experiments is the uncertainty in the actual subsidence rate during the transition (Bretherton and Pincus, 1995) and the large temporal and spacial variability of the divergence in the ECMWF reanalysis data.

Moreover, recent research (De Roode and Van der Dussen, 2010; Sandu and Stevens, 2011) points out that lowering the subsidence rate tends to delay cloud break-up. This effect opposes earlier hypotheses (Bretherton and Pincus, 1995), stating that the decreasing subsidence observed during ASTEX actually led to the rapid break-up of the cloud layer, through the increase of boundary layer decoupling.

Figure 3 shows the prescribed large scale divergence as a function of time for all four of the simulations that

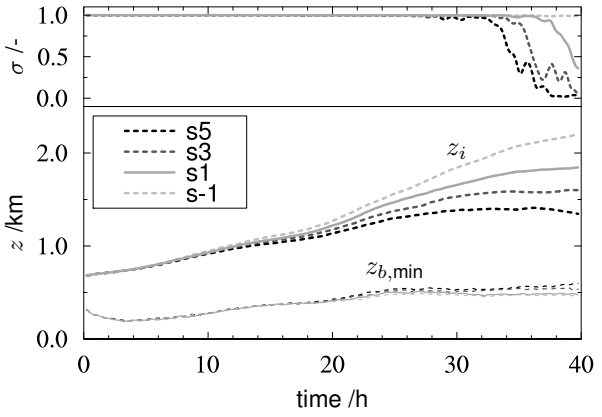


**FIG. 4:** The total cloud cover $\sigma$ (top panel) as well as the inversion height $z_i$ and minimum cloud base height $z_{b,\min}$ (bottom panel) for the divergence sensitivity experiments as defined in Figure 3. A running averaging filter with a width of 30 min is used to slightly smoothen the results.

were performed. All simulations start with a divergence of $5 \times 10^{-6}\,\mathrm{s}^{-1}$, but differ in the rate of change with time. Experiment 's1' is identical to the reference simulation and is indicated with a solid grey line. The dashed lines are the sensitivity experiments. The darker the line color, the higher the large scale divergence, i.e. the stronger the subsidence. The vertical velocity $\overline{w}$ is calculated by:

$$\overline{w(z)} = -Dz \qquad \text{for } z \leq 1600\,\mathrm{m} \tag{22}$$

and is kept constant above.

Figure 4 gives an overview of the simulation results by showing the total cloud cover as a function of time in the upper panel and in the lower panel the inversion height and the minimum cloud base height as a function of time. From the cloud cover plot, it is clear that the stronger the subsidence (darker lines) the earlier the stratocumulus cloud breaks up. The difference in transition time is significant, up to 25 %.

The bottom panel in Figure 4, reveals a large difference in the inversion height among the simulations. Minimum cloud base height, on the other hand, is hardly influenced by the divergence perturbation. The deeper boundary layer in cases with a lower large scale divergence is of course expected, since the subsidence rate is directly related to the inversion height via Eq. (12). For the cases considered here, the direct effect of a decrease in the divergence account for 50 to 70 % of the total increase in $z_i$. The additional increase of the boundary layer depth is due to an increase in the entrainment rate $w_e$ during the second part of the transition, which is shown in Figure 5a. Intuitively, that would lead to a more rapid drying of the cloud layer. That this is not the case is shown by Figure 5b. This could mean two things: 1) the additional entrainment does not lead to larger entrainment fluxes, due to differences in the inversion jumps of $q_T$ and $\theta_L$, or 2) the additional drying and heating due to larger entrainment fluxes is compensated for by changes in the contribution

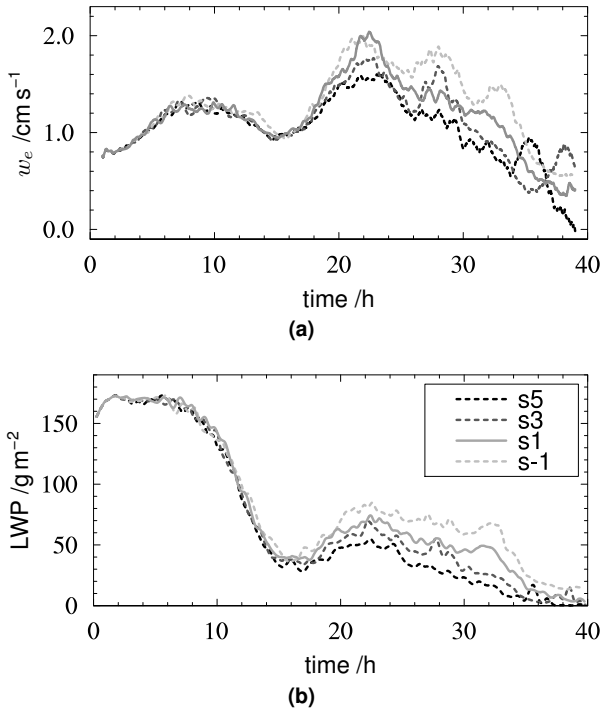


**FIG. 5:** The entrainment rate (a) and the LWP (b), for each of the divergence sensitivity experiments as defined in Figure 3. A running averaging filter with a width of respectively 2 h and 30 min is used to reduce the noise.

due to other processes.

The inversion jump of a variable $\varphi$ is defined as the difference between $\varphi$ just above ($^+$) and just below ($^-$) the inversion:

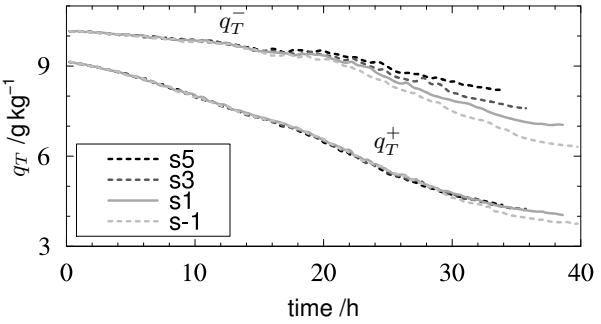


**FIG. 6:** The humidity just above and just below the inversion layer (respectively $q_T^+$ and $q_T^-$) as a function of time, for each of the divergence sensitivity experiments as defined in Figure 3. The timeseries have been truncated at the moment the total cloud cover drops below 70 %.

$$\Delta_i \varphi = \varphi^+ - \varphi^-, \tag{23}$$

the values of which were again determined based on the level at which the vertical gradient drops to a certain percentage of the maximum gradient, at which the inversion is located.

**Tab. 1:** The difference in LWP tendency of each case with respect to s5 (indicated by $\Delta$), according to Eq. (20). The value shown is an average over hours 16 to 22.

| | $\Delta$Base | $\Delta$Div | $\Delta$Ent | $\Delta$Rad | $\Delta$Prec | $\Delta$Total |
|---|---|---|---|---|---|---|
| s5 | 0 | 0 | 0 | 0 | 0 | 0 |
| s3 | +2 | +1 | +1 | 0 | 0 | +4 |
| s1 | +7 | +2 | -4 | -1 | +1 | +5 |
| s-1 | +10 | +3 | -3 | -1 | +2 | +11 |

For $\varphi = q_T$, these values have been plotted in Figure 6. The increase of the boundary layer height by entrainment, combined with the prescribed lapse rate of $q_T$ in the free atmosphere causes $q_T^+$ to decrease in time. Figure 6 shows that the rate of this decrease is hardly affected by changing the divergence.

The value of $q_T$ just below the inversion on the other hand, is significantly lower in the cases with lower subsidence. This is an effect of the increased depth of the boundary layer and the subsequent additional decoupling, as was found from models and observations by Park et al. (2004) and by Wood and Bretherton (2004). Due to this effect, the magnitude of the inversion jump of $q_T$ (and similarly that of $\theta_L$) tends to be smaller at lower subsidence rates.

The increase of the entrainment rate as the subsidence is decreased, dominates over the decrease in the magnitude of the inversion jumps, such that the entrainment fluxes, as defined by Eq. (11), increase. The first term on the rhs of Eq. (21b), therefore, causes additional cloud thinning in case of decrease of the divergence. The second term on the rhs of this equation, on the other hand, causes additional thickening of the cloud layer for a decreased divergence. Because of these competing effects, the net change in the entrainment term is modest for the performed sensitivity experiments. This is confirmed by the plots of the time series of the entrainment contributions for the simulations, shown in Figure 7a. A similar plot for the contribution of the turbulent fluxes of $q_T$ and $\theta_L$ at stratocumulus cloud base height is shown in Figure 7b.

According to the LWP time series in Figure 5b, the period in which the LWP differences develop is between hours 16 to 22. The average tendencies due to entrainment and due to cloud base turbulent fluxes are indicated in Figure 7 by horizontal lines. Furthermore, Table 1 contains, for each term of Eq. 21, the difference as compared to simulation s5, again averaged over hours 16 to 22.

In general, the differences between the cases are small. The change in the cloud base flux tendency is largest for all cases and constitutes most of the net change in the LWP tendency.

More quantitatively, the average difference in LWP tendency between case s-1 (lowest subsidence, light grey) and s5 (highest subsidence, black) during the period mentioned before is $11\,\mathrm{g\,m^{-2}\,h^{-1}}$, resulting in an integrated difference between the cases of over $60\,\mathrm{g\,m^{-2}}$.

Differences due to radiation and precipitation are small during this period (see Table 1), since these processes depend mostly on the LWP. Especially during the first part of the period, the LWP differences are small. The differences in the contribution of the divergence are slightly larger, at about $3\,\mathrm{g\,m^{-2}\,h^{-1}}$.

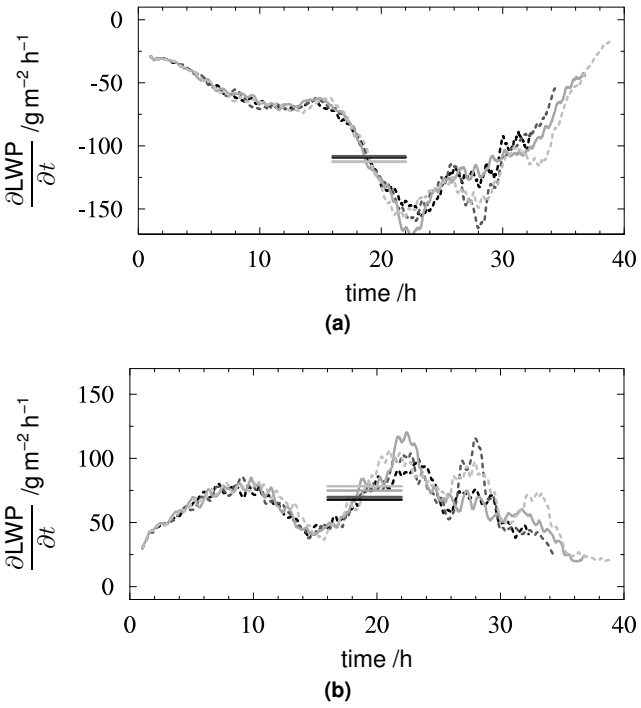


**FIG. 7:** The contributions of entrainment (a) and of cloud base fluxes (b) to the liquid water path tendency, according to Eqs. (21b) and (21a) respectively. The horizontal black lines indicate the average tendencies during hours 16 to 22.

## 4. DISCUSSION AND CONCLUSIONS

A more in-depth analysis is presented of the results of the combined GASS/EUCLIPSE model intercomparison case based on the ASTEX field campaign, which were obtained using DALES. The set-up of this case and the comparison of the results of several LES models with observations will be described in DR12.

A tendency equation is derived for the cloud liquid water path. By reordering the terms of this equation, the tendencies due to each of the following physical processes can be extracted: entrainment, cloud base fluxes, divergence, radiation and precipitation.

The magnitude of each of the terms of the LWP tendency equation is diagnosed from the LES results. It is shown that the contributions of the separate processes cancel to a high degree, resulting in a relatively small net LWP tendency. For larger scale models or single column model versions of these models, which rely heavily on parametrisation in this regime, this means that making a small error in any of the processes leads to an unrealistic tendency of the cloud layer thickness. The fact that the terms cancel to such an extent, on the other hand, could possibly be used to check the results of parametrisations to find possible defects. It furthermore shows that the links between the parametrised processes should be sufficiently strong, in order for the net tendency to respond correctly to changes in, for instance, the surface fluxes or in precipitation.

In this respect, it is interesting to apply the LWP tendency equation on the results of other LES models that participate in the EUCLIPSE model intercomparison case of which this research is part. This could shed more light on questions regarding the influence of differences in parametrised precipitation or radiative cooling/warming rates on the LWP.

In addition to the standard LES simulation of the ASTEX transition, three sensitivity simulations are performed, to investigate the effect of changes to the large scale divergence. The simulations show that a decrease of the large scale divergence tends to slow down the pace of the transition, resulting in a delay of the break-up of the stratocumulus cloud layer. This confirms earlier results by De Roode and Van der Dussen (2010) and Sandu and Stevens (2011).

The LWP budget analysis is applied to each of the sensitivity experiments, in order to get a better idea of which of the processes is responsible for the difference in LWP tendency.

Even though the differences in the different terms of the LWP tendency equation among the cases are generally very small, it is clear that most of the change of the LWP tendency, resulting from a perturbation of the divergence, is due to a change in the contribution of the turbulent fluxes of $q_T$ and $\theta_L$ at cloud base, i.e. the cloud base fluxes have a stronger cloud thickening effect in the lower divergence cases. Further research is required in order to be able to answer the question of how the decoupling of the boundary layer turbulence is linked to the development of multiple layers in an initially well-mixed boundary layer.

As a result of the decrease of the divergence, the entrainment rate is shown to increase significantly. The additional drying and warming is, however, limited, as the inversion jumps of $q_T$ and $\theta_L$ tends to be smaller as a result of the increased decoupling (of the mean state profiles), which is typically found in deeper boundary layers. Therefore, the magnitude of the change in the LWP tendency due to entrainment is approximately three times as small as that of cloud base fluxes. The radiative and precipitative contributions change only little and the changes are likely only a reaction to the differences in the LWP.


## ACKNOWLEDGMENTS

The investigations were done as part of the European Union Cloud Intercomparison, Process Study & Evaluation Project (EUCLIPSE) project, funded under Framework Program 7 of the European Union. The work was sponsored by the National Computing Facilities Foundation (NCF) for the use of supercomputer facilities.


## A. PARTIAL DERIVATIVES OF LIQUID WATER CONTENT

Equations for the evaluation of the partial derivatives of $q_L$ with respect to $q_T$ and $\theta_L$ can be found using the definitions of these variables. An expression should be found for:

$$\left(\frac{\partial q_L}{\partial q_T}\right)_{\theta_L, z_i} \quad \text{and for} \quad \left(\frac{\partial q_L}{\partial \theta_L}\right)_{q_T, z_i} \tag{A-1}$$

### A.1 *Total humidity*

Firstly, the definition of $\theta_L$ is written in its differential form:

$$\mathrm{d}\theta_L = \mathrm{d}\theta - \frac{L_v}{\Pi c_p}\mathrm{d}q_L, \tag{A-2}$$

where $\Pi = \Pi(p)$ is the Exner function. Now, because $\theta_L$ is kept constant, the lhs of Eq. (A-2) is zero, which, after rewriting, gives:

$$\mathrm{d}T = \frac{L_v}{c_p}\mathrm{d}q_L. \tag{A-3}$$

In a saturated environment $q_T$ can be written as the sum of the saturation specific humidity $q_s$ and the liquid water content. In its incremental form, this can be written as:

$$\mathrm{d}q_T = \mathrm{d}q_s + \mathrm{d}q_L. \tag{A-4}$$

Equation (A-3) can now be used to substitute out $\mathrm{d}q_L$ in this equation, giving:

$$\mathrm{d}q_T = \mathrm{d}q_s + \frac{c_p}{L_v}\mathrm{d}T = \left(1 + \frac{c_p}{L_v\gamma}\right)\mathrm{d}q_s. \tag{A-5}$$

where $\gamma$ is defined as:

$$\gamma \equiv \frac{\partial q_s}{\partial T} = \frac{L_v q_s}{R_v T^2}. \tag{A-6}$$

Here, the second equality is given by the Clausius-Clapeyron relation. Using this expression to substitute out $\mathrm{d}q_s$ in Eq. (A-4) and rearranging the terms gives:

$$\mathrm{d}q_T = \left(\frac{L_v\gamma}{c_p + L_v\gamma}\right)\mathrm{d}q_T + \mathrm{d}q_L, \tag{A-7}$$

which can be solved for $\mathrm{d}q_T$. The partial derivative can then be written as:

$$\left(\frac{\partial q_L}{\partial q_T}\right)_{\theta_L, z_i} = \eta, \tag{A-8}$$

where $\eta$ is defined as:

$$\eta \equiv \frac{c_p}{c_p + L_v\gamma}. \tag{A-9}$$

This $\eta$ can be interpreted as an efficiency at which increments in $q_T$ are converted to $q_L$. Figure A-1a shows the values of $\eta$ for a relevant range of temperatures and pressures.

### A.2 *Liquid water potential temperature*

Using the definition of the potential temperature $\theta$, the incremental form can be written as:

$$\mathrm{d}\theta = \frac{\mathrm{d}T}{\Pi} = \frac{1}{\Pi}\frac{\partial T}{\partial q_s}\mathrm{d}q_s. \tag{A-10}$$

Furthermore, in a saturated environment, at constant $q_T$:

$$\mathrm{d}q_s = -\mathrm{d}q_L. \tag{A-11}$$

Now Eqs. (A-10) and (A-11) can be used in Eq. (A-2) to give:

$$\mathrm{d}\theta_L = -\frac{1}{\Pi}\left(\frac{1}{\gamma} + \frac{L_v}{c_p}\right)\mathrm{d}q_L. \tag{A-12}$$

Then, the partial derivative of $q_L$ with respect to $\theta_L$ can be written:

$$\left(\frac{\partial q_L}{\partial \theta_L}\right)_{q_T, z_i} = -\Pi\gamma\eta, \tag{A-13}$$

with $\eta$ as defined by Eq. (A-9). Typical values for $-\Pi\gamma\eta$ for a relevant range of temperatures and pressures are shown in Figure A-1b.

## B. SATURATION SPECIFIC HUMIDITY AS A FUNCTION OF HEIGHT

Since $q_s = f(T, p)$ the following can be written using partial differentiation:

$$\frac{\partial q_s}{\partial z} = \left(\frac{\partial q_s}{\partial T}\right)_p \frac{\partial T}{\partial z} + \left(\frac{\partial q_s}{\partial p}\right)_T \frac{\partial p}{\partial z} \tag{B-1}$$

Rewriting the first term gives:

$$\left(\frac{\partial q_s}{\partial T}\right)_p \frac{\partial T}{\partial z} = \gamma\Gamma_T \tag{B-2}$$

where $\Gamma_T$ is the lapse rate of temperature. Since Eq. (B-1) should be evaluated incloud, $\Gamma_T$ is the saturated adiabatic lapse rate, approximated by:

$$\Gamma_{T,s} \approx -\frac{g}{c_p} - \frac{L_v}{c_p}\frac{\partial q_s}{\partial z}, \tag{B-3}$$

in which $q_v$ in the partial derivative has been replaced by $q_s$.
To rewrite the second term on the right hand side, the following equation can be used for $q_s$ (e.g. Stull, 1988):

$$q_s \approx \frac{\varepsilon e_s}{p}. \tag{B-4}$$

Here $e_s$ is the saturation pressure and $\varepsilon = R_d/R_v$ is the ratio of the gas constant of water vapour to that of dry air. Differentiating this equation with respect to $p$ results in:

$$\frac{\partial q_s}{\partial p} = -\frac{q_s}{p}. \tag{B-5}$$

Furthermore, by assuming that the atmosphere is in hydrostatic equilibrium:

$$\frac{\partial p}{\partial z} = -\rho g \approx -\frac{pg}{R_d T}. \tag{B-6}$$

Substitution of Eqs. (B-2), (B-3), (B-5) and (B-6) into Eq. (B-1) gives:

$$\left(1 + \frac{\gamma L_v}{c_p}\right)\frac{\partial q_s}{\partial z} = -\frac{g\gamma}{c_p} + \frac{g q_s}{R_d T}. \tag{B-7}$$

Rewriting finally results in:

$$\frac{\partial q_s}{\partial z} = g\eta\left(\frac{q_s}{R_d T} - \frac{\gamma}{c_p}\right). \tag{B-8}$$

When Teten's formula is used to approximate $q_s(T, p)$, this equation can be evaluated at each pressure and temperature. In the relevant temperature and pressure range, the lapse rate is relatively constant at approximately $-2\,\mathrm{g\,kg^{-1}\,km^{-1}}$.

## References


Albrecht BA, Bretherton CS, Johnson D, Scubert WH, and Frisch AS, 1995: The atlantic stratocumulus transition experimentent–ASTEX. *Bull. Amer. Meteor. Soc.*, **76 (6)**, 889–904.

Bougeault P, 1985: The diurnal cycle of the marine stratocumulus layer: A higher-order model study. *J. Atmos. Sci.*, **42 (24)**, 2826–2843.

Bretherton CS, Austin P, and Siems ST, 1995: Cloudiness and marine boundary layer dynamics in the ASTEX lagrangian experiments. part II: Cloudiness, drizzle, surface fluxes, and entrainment. *J. Atmos. Sci.*, **52 (16)**, 2724–2735.

Bretherton CS, Krueger SK, Wyant MC, Bechtold P, Van Meijgaard E, Stevens B, and Teixeira J, 1999: A GCSS boundary-layer cloud model intercomparison study of the first ASTEX Lagrangian experiment. *Bound.-Layer Meteor.*, **93 (3)**, 341–380.

Bretherton CS and Pincus R, 1995: Cloudiness and marine boundary layer dynamics in the ASTEX lagrangian experiments. part I: Synoptic setting and vertical structure. *J. Atmos. Sci.*, **52 (16)**, 2707–2723.

Brient F and Bony S, 2012: Interpretation of the positive low-cloud feedback predicted by a climate model under global warming. *Climate Dynamics*, 1–17.

Ciesielski PE, Schubert WH, and Johnson RH, 1999: Large-scale heat and moisture budgets over the ASTEX region. *J. Atmos. Sci.*, **56 (18)**, 3241–3261.

De Roode SR and Duynkerke PG, 1996: Dynamics of cumulus rising into stratocumulus as observed during the first lagrangian experiment of ASTEX. *Quart. J. Roy. Meteor. Soc.*, **122 (535)**, 1597–1623.

De Roode SR and Duynkerke PG, 1997: Observed lagrangian transition of stratocumulus into cumulus during ASTEX: Mean state and turbulence structure. *J. Atmos. Sci.*, **54 (17)**, 2157–2173.

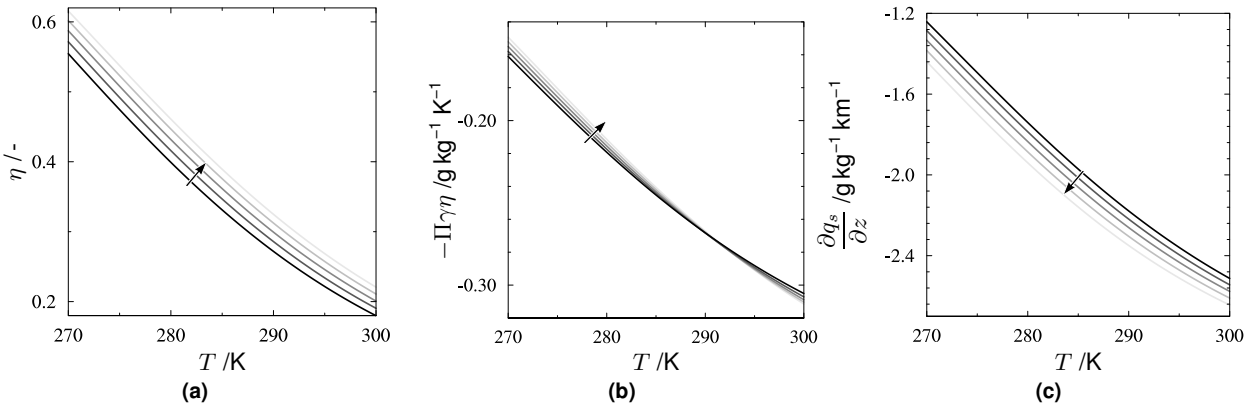


**FIG. A-1:** Values of $\eta$ (Eq. A-9) (a), $-\Pi\gamma\eta$ (Eq. A-13) (b) and of the lapse rate of $q_s$ (Eq. B-8) (c) for a relevant range of temperatures and pressures. The arrows point towards increasing pressure (from 700 to 900 hPa with 50 hPa increments).


De Roode SR and Van der Dussen JJ, 2010: Large-eddy simulation of a stratocumulus to cumulus cloud transition as observed during ASTEX. *Proceedings of the 19th Symp. Bound.-Layers and Turbulence*, Keystone, URL http://ams.confex.com/ams/pdfpapers/172386.pdf.

Duynkerke PG, et al., 1999: Intercomparison of three- and one-dimensional model simulations and aircraft observations of stratocumulus. *Bound.-Layer Meteor.*, **92 (3)**, 453–487.

Heus T, et al., 2010: Formulation of the dutch atmospheric large-eddy simulation (dales) and overview of its applications. *Geosci. Model Dev.*, **3 (2)**, 415–444.

Martin GM, Johnson DW, Rogers DP, Jonas PR, Minnis P, and Hegg DA, 1995: Observations of the interaction between cumulus clouds and warm stratocumulus clouds in the marine boundary layer during ASTEX. *J. Atmos. Sci.*, **52 (16)**, 2902–2922.

Park S, Leovy CB, and Rozendaal MA, 2004: A new heuristic lagrangian marine boundary layer cloud model. *J. Atmos. Sci.*, **61 (24)**, 3002–3024.

Randall DA, 1984: Stratocumulus cloud deepening through entrainment. *Tellus A*, **36A (5)**, 446–457.

Sandu I and Stevens B, 2011: On the factors modulating the stratocumulus to cumulus transitions. *J. Atmos. Sci.*, **68 (9)**, 1865–1881.

Sandu I, Stevens B, and Pincus R, 2010: On the transitions in marine boundary layer cloudiness. *Atmos. Chem. Phys.*, **10 (5)**, 2377–2391.

Stull R, 1988: *An Introduction to Boundary Layer Meteorology*. Kluwer Academic Publishers.

Svensson G, Tjernstrm M, and Korain D, 2000: The sensitivity of a stratocumulus transition: Model simulations of the ASTEX first Lagrangian. *Bound.-Layer Meteor.*, **95 (1)**, 57–90.

Turton JD and Nicholls S, 1987: A study of the diurnal variation of stratocumulus using a multiple mixed layer model. *Quart. J. Roy. Meteor. Soc.*, **113 (477)**, 969–1009.

Wood R and Bretherton CS, 2004: Boundary layer depth, entrainment, and decoupling in the cloud-capped subtropical and tropical marine boundary layer. *J. Climate*, **17 (18)**, 3576–3588.

Zhang M, Bretherton C, Webb M, and Siebesma A, 2010: CFMIP-GCSS intercomparison of large eddy models and single column models (CGILS). *GEWEX News*, **20**, 6–8.